Functional Topography of Rod and Cone Photoreceptors in Macaque Retina Determined by Retinal Densitometry

Gen Hanazono,[1,2] *Kazushige Tsunoda,*[1,2] *Yoko Kazato,*[1,2] *Wataru Suzuki,*[1,2,3] *and Manabu Tanifuji*[2]

Purpose. The purpose of this study is to determine the topography of bleaching in rods, middle/long-wavelength (M/L) and short-wavelength (S) cones in the macaque retina by using a modified retinal densitometry technique.

Methods. A modified commercial digital fundus camera system was used to measure continuously the intensity of the light reflectance during bleaching with band pass lights in the ocular fundus of three adult Rhesus monkeys (Macaca mulatta) under general anesthesia. The topography of bleaching in rods, M/L-, and S-cones was obtained separately by considering the characteristic time course of the reflectance changes, depending on the wavelengths of light and retinal locations.

Results. The distribution of M/L-cones response had a steep peak at the foveal center and was elongated horizontally. The distribution of rod responses was minimum at the foveal center and maximum along a circular region at the eccentricity of the optic disc. The distribution of S-cone responses was highest at the fovea and was excavated centrally. There was a circular region with the maximal responses at 0.38 to 1.0 degrees from the foveal center.

Conclusions. With the current imaging technique, not only the steep peak of the M/L-cone responses at the fovea, but the ring-shaped distribution of rod responses in the periphery and the central reduction of S-cone response could be determined with good resolution. (*Invest Ophthalmol Vis Sci.* 2012;53:2796–2803) DOI:10.1167/iovs.11-9252

The human visual system is a duplex system, consisting of a rod system for scotopic conditions and a cone system for photopic conditions. Three types of cones mediate color vision; long (L), middle (M), and short (S) wavelength-sensitive cones. The distribution of the photoreceptors has been well investigated on postmortem eyes of humans and macaques.[1–9] These studies reported the anatomical densities of the different types of photoreceptors, but the results did not necessarily reflect their functional properties. Psychophysical experiments also have been used to assess photoreceptor function.[10–15] However, the results reflect not only the retinal function, but the visual function from the photoreceptors to the visual cortex.

Approximately 50 years ago, the time course of the bleaching of photopigments was determined quantitatively by measuring the reflectance changes during bleaching and regeneration of the visual pigments in human retinas.[16–22] This method, retinal densitometry, was used to determine the in vivo kinetics of the photopigments of cones and rods quite accurately. The spatial distribution of the reflectance changes was determined later by examining images obtained by either a fundus camera or a scanning laser ophthalmoscope (SLO), that is, imaging fundus reflectometry.[23–33] With these techniques, the distribution of photoreceptors was mapped objectively and non-invasively as bleach-derived light reflectance changes in normal and diseased eyes. However, the responses of the different types of photoreceptors, especially rods and S-cones, could not be segregated accurately because the response time courses were not monitored accurately.

We developed a new retinal densitometry system that can measure the retinal reflectance changes continuously after bleaching with band pass lights in anesthetized rhesus monkeys. We found that the time course of the reflectance changes depended not only on the wavelength of light but on the retinal location. By using such characteristics, the topography of bleaching in rods, M/L-, and S-cones could be obtained separately. The circular region of the maximal rod responses and the reduction of S-cone responses in the center were determined functionally with good spatial resolution.

Methods

The experiments were performed on three adult Rhesus monkeys (Macaca mulatta). Following an intramuscular injection of atropine sulfate (0.08 mg/kg), the monkeys were anesthetized with droperidol (0.25 mg/kg) and ketamine (5.0 mg/kg), and then paralyzed with vecuronium bromide (0.1 mg/ kg/ hour). To block pain, fentanyl citrate (0.83 μg/kg/h) was infused intravenously continuously throughout the experiments. The animals were ventilated artificially with a mixture of 70% N_2O, 30% O_2, and 1.0–1.5% of isoflurane. The electroencephalograms (EEGs), electrocardiograms (ECGs), expired CO_2, and rectal temperature were monitored continuously throughout the experiments. Before the recordings, the pupils were dilated fully with topical tropicamide (0.5%) and phenylephrine hydrochloride (0.5%). The experimental protocol was approved by the Experimental Animal Committee of the RIKEN Institute, and all experimental procedures were carried out in accordance with the guidelines of the RIKEN Institute and the ARVO Statement for the Use of Animals in Ophthalmic and Vision Research.

From the [1]Laboratory of Visual Physiology, National Institute of Sensory Organs, Tokyo, Japan, [2]Laboratory for Integrative Neural Systems, RIKEN Brain Science Institute, Saitama, Japan, and [3]Department of Ultrastructural Research, National Institute of Neuroscience, National Center of Neurology and Psychiatry, Tokyo, Japan.

Supported in part by research grants from the Ministry of Health, Labor and Welfare, Japan and Grant-in-Aid for Scientific Research, Japan Society for the Promotion of Science, Japan.

Submitted for publication December 6, 2011; revised February 20, 2012; accepted March 7, 2012.

Disclosure: **G. Hanazono**, None; **K. Tsunoda**, None; **Y. Kazato**, None; **W. Suzuki**, None; **M. Tanifuji**, None

Corresponding author: Kazushige Tsunoda, Laboratory of Visual Physiology, National Institute of Sensory Organs, Japan, 2-5-1, Higashigaoka, Meguro-ku, Tokyo, 152-8902, Japan; Telephone 03-3411-0111, Fax 03-3411-0185; tsunodakazushige@kankakuki.go.jp.

Investigative Ophthalmology & Visual Science, May 2012, Vol. 53, No. 6

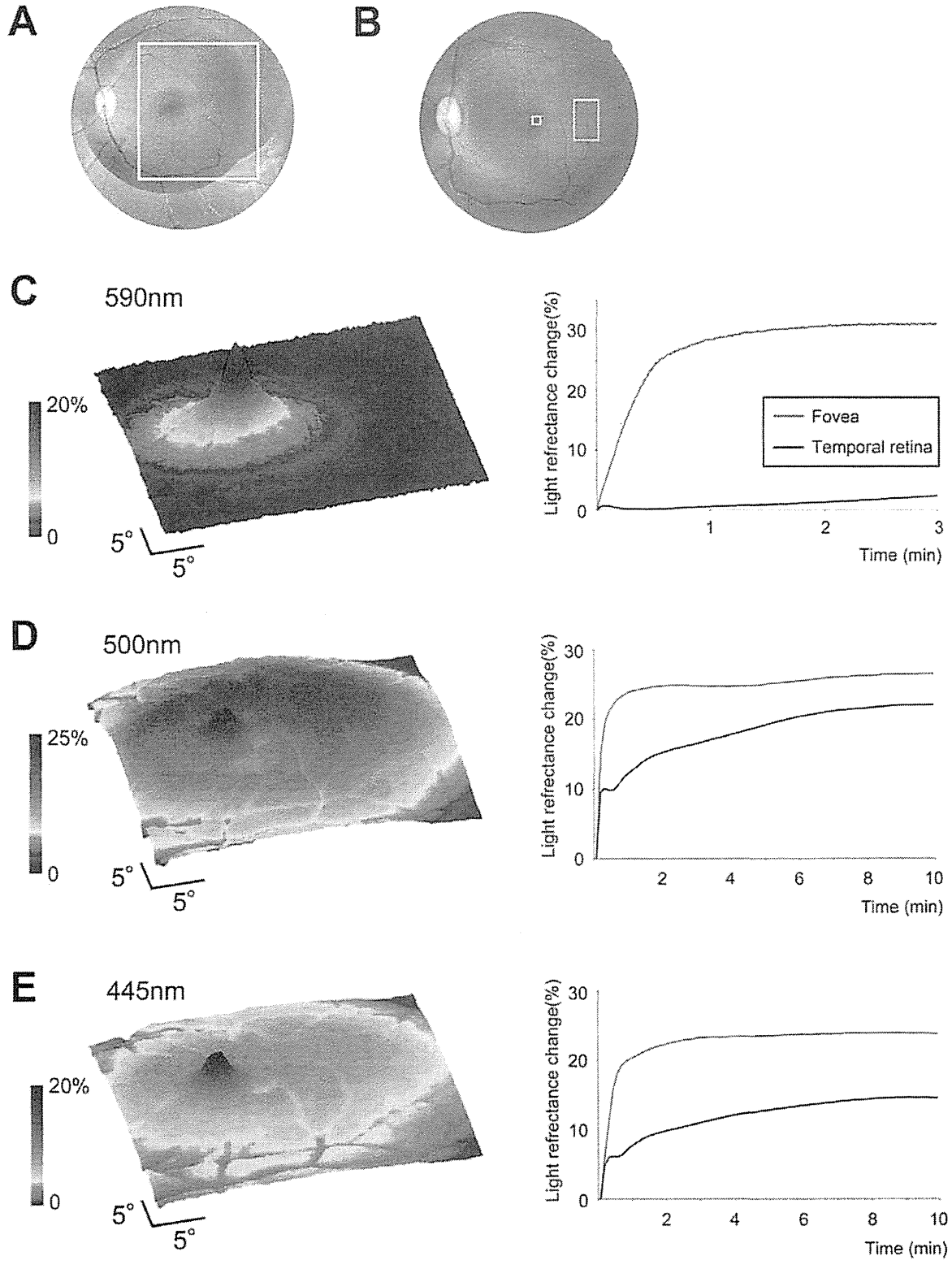

FIGURE 1. Bleach-induced light reflectance changes in retina by different wavelengths of light. (A, B) Regions in the macaque retina for the topographic (A) and time course analyses (B). A small square in B indicates the location of the fovea and a rectangle indicates the location of the temporal retina. (C–E) Pseudo-colored topographic map of the bleach-induced light reflectance changes (*left*), and time course in the fovea and temporal retina with high intensity light of 5.35 log phot. td for 590 nm (C), 6.54 log scot. tld for 500 nm (D), and 4.58 log phot. td for 445 nm (*right*) (E). Color scales indicate the reflectance changes (%) at the completion of each recording period relative to the reflectance at the beginning. Red lines indicate the time course at the fovea and blue lines for the temporal retina. Data from Monkey 1 are presented.

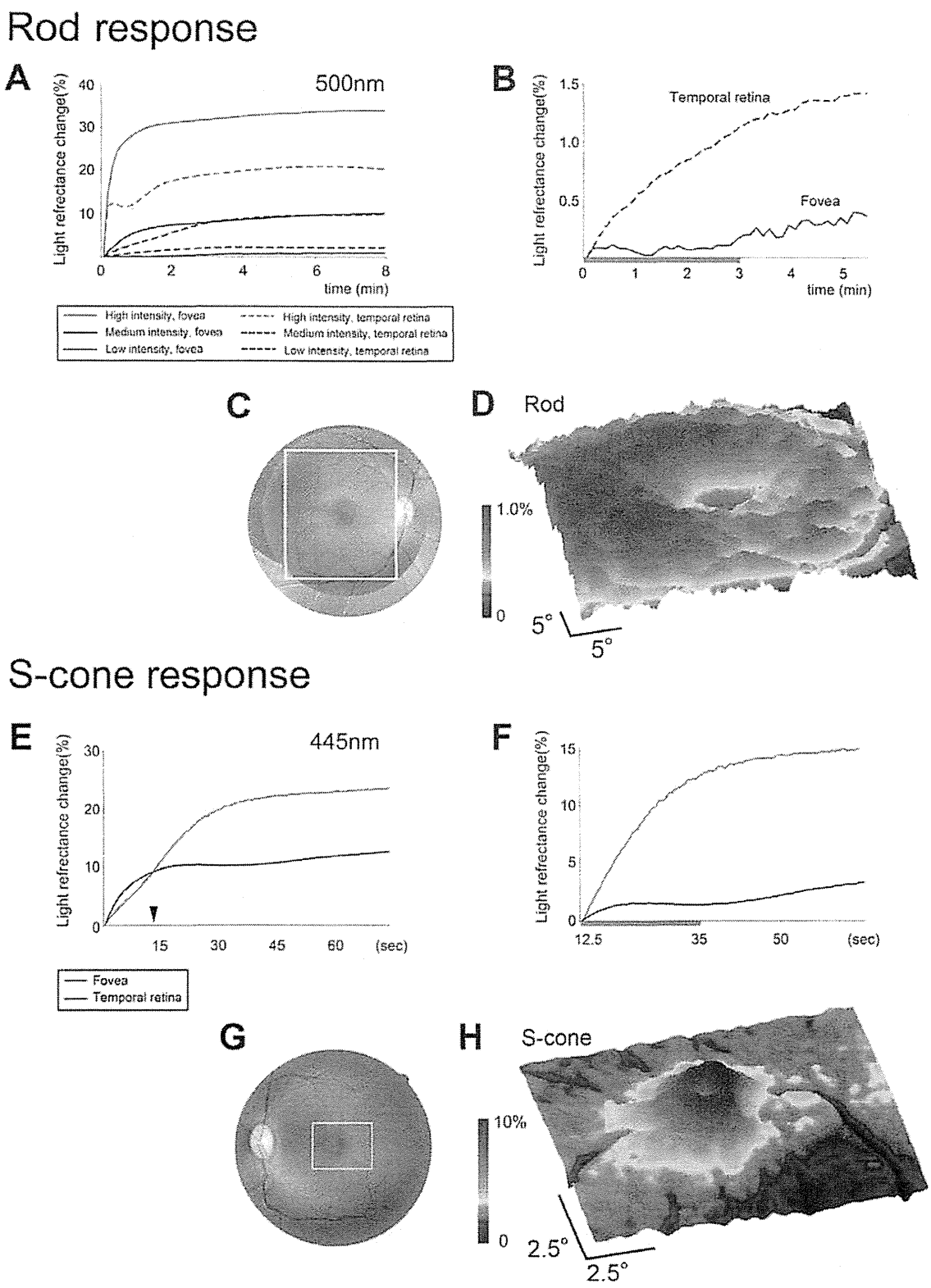

FIGURE 2. Time-course analyses for the rod (A–D) and S-cone (E–H) responses. (A) Time courses for 500 nm at three different intensities; 6.54 log scot. tld for strong, 5.14 log scot. tld for medium, and 4.73 log scot. tld for weak intensity. Time course at the fovea is represented by solid lines and those at the temporal retina by dotted lines. (B) Expanded image of the time course for the weak 500 nm light (4.73 log scot. tld) for the initial five minutes. The response at the fovea remains flat during the initial three minutes. (C, D) Reflectance topographic map for weak 500 nm light (4.73 log scot. tld) during the initial three minutes (D) measured in the posterior-pole region in (C). The color scale indicates the reflectance changes (%) at 3 minutes. (E, F) Expanded time course for the 455 nm light for the initial 75 seconds (E), and re-plotted reflectance changes relative to the

Retinal Densitometry System and Data Analyses

A modified commercial digital fundus camera system (NM-1000, Nidek, Aichi, Japan) was used to observe and measure continuously the light reflectance changes from the ocular fundus. The fundus images were recorded with a CCD video camera (PX-30BC, Primetech Engineering, Tokyo, Japan), and the images were digitized with an IBM/PC-compatible computer equipped with a video frame grabber board (Corona II, Matrox, Quebec, Canada; gray-level resolution 10 bits, spatial resolution 640 × 480, temporal resolution 1/30 seconds). The optical pathway was modified to illuminate the entire posterior pole region homogeneously for 35 degrees in diameter by inserting a neutral density filter within the optical pathway that was conjugate to the retina. The density of the filter was the highest at the center and decreased gradually toward the periphery to compensate for the highest luminance along the optical axis, which is characteristic to commercial fundus cameras. With this filter, the differences of the estimated retinal luminances within the region of interest were within ± 10%.

Following dark adaptation for one hour, the fundus was illuminated continuously in the dark room with the light from a halogen lamp filtered through one of the three band pass interference filters: blue ($\lambda_{max} = 445 \pm 30$ nm) for S-cone, green ($\lambda_{max} = 500 \pm 15$ nm) for rods, and yellow ($\lambda_{max} = 590 \pm 15$ nm) for M/L-cones. Because the maximum absorption of the M and L cones was close, that is 535 nm for M-cones and 565 nm for L-cones, and differentiation between M- and L-cones in this method was technically difficult, we did not aim to segregate the response topography of these two types of cones. These cones thus were referred to as M/L-cones in this study.

The bleaching of the photopigments was measured as increases in light reflectance from the ocular fundus, that is a brightening. The time course of the reflectance changes was calculated as follows. The gray-scale values of the images obtained after the stimulus were divided, pixel by pixel, by those obtained during a 0.5-second period at the beginning of the trial. This ratio was rescaled to 256 levels of gray-scale resolution to show the stimulus-induced reflectance changes. In each trial, the reflectance was recorded for as long as 11 minutes, which is the maximum recording duration possible in our computer system. Spatial averaging (3 × 3 pixels, i.e. 0.15 × 0.15 degrees, for mapping M/L- and S-cones, or 5 × 5 pixels, i.e. 0.25 × 0.25 degrees, for rods) was performed to build up topographies of retinal responses.

For measuring the rod reflectance changes of the peaks not located in the macular region, six trials were performed consecutively to measure the light reflectance changes in different retinal locations (Fig. 3B). The topographies of these trials were merged to map the responses over 40 degrees in diameter.

We made measurements on three monkeys, and the results with unwanted physiological artifacts, such as the large decrease of reflectance along the vessels due to absorption by hemoglobin and pulsation-induced reflectance changes at the edge of the optic disk, were excluded from the response topographies.

Results

Topography and Time Course of Maximum Bleaching for Each Band Pass Filter

We bleached the retina with different wavelengths of light, and the topographic distribution of the bleaching patterns with yellow (5.35 log phot. td), green (6.54 log scot. tld) and blue (4.58 log phot. td) are shown in Figure 2. The time course of reflectance changes at the foveal area of 1.75 degrees in diameter and temporal retina 15.0 degrees from the center are shown. The light through the yellow (590 nm) filter bleached the M- and L- cones exclusively,[18,20,34,35] and the changes in the reflectance represented a combination of M/L-cones. The topographic profile showed a high and steep peak of light reflectance increase at the foveal center, which decreased gradually toward the periphery (Fig. 1C).

The green (500 nm) wavelength generally bleaches rods, S-, and M/L-cones,[18,20,34,35] and the topographic changes in reflectance caused by 500 nm light represents the bleaching of all types of photoreceptors. There were high peaks of light reflectance changes at the fovea and the circular region surrounding the macula at an eccentricity of the optic disc (Fig. 1D). The time course of the light reflectance changes was monophasic at the fovea, but biphasic at the temporal retina. The biphasic time course was observed at all retinal locations except for the fovea, and can be explained by the bleaching processes of rod photoreceptors, that is bleaching of 11-cis-retinal to Meta-II intermediates (peak 380 nm) for the initial phase and the bleaching of Meta-III intermediates (peak 465 nm) to all-transretinal and opsin in the late phase.[36,37] These findings indicated that the response topography at the fovea is dominated by bleaching of cones and that in the peripheral region is dominated by bleaching of rods.

Both the S-cones and rods are sensitive to 445 nm,[18,20,34,35] and the topographic changes in the reflectance pattern after bleaching with the green (445 nm) filter represents mainly the bleaching of both rods and S-cones. However, the M/L cones also absorb this wavelength. As with bleaching with 500 nm, the bleaching profile showed that there were peaks of light reflectance changes at the fovea and the circular region surrounding the macula (Fig. 1E). However, the foveal peak was not steep as with 590 or 500 nm but more rounded. This indicated that the reflectance topography at the fovea was not dominated by bleaching of M/L-cones, which should be the maximum at the foveal center. The time course of the light reflectance changes was monophasic at the fovea but biphasic at the temporal retina, as it was with 500 nm. This indicated that the reflectance topography in the peripheral region is dominated by the bleaching of rods.[36,37]

Mapping Rod and S-Cone Responses Based on Bleaching Time Course

The time courses of the reflectance changes during bleaching by 500 nm of different intensities are shown in Figure 2A. With high intensity of 6.54 log scot. tld, the reflectance changes were greater at the fovea (39.9%) than at the temporal retina (20.4%) 8 minutes following the onset of bleaching (Fig. 2A, red line). With low intensity light of 4.73 log scot. tld, the light reflectance changes were lower at the fovea (1.03%) than at the temporal retina (2.28%, Fig. 2A, black line). In addition, during the initial three minutes of bleaching with low intensity light, the foveal response was minimal and remained at 0.1% (Fig. 2B, solid line). This indicated that bleaching of rod photoreceptors could be isolated by measuring the reflectance changes with low light intensity during the initial three minutes. Thus, the topographic distribution of the bleaching of rods could be obtained, and it had a donut-shaped circular

reflectance value at 12.5 sec after the onset (*arrowhead* in **E**) (**F**). The response at the temporal retina remains almost flat between 12.5 to 35.0 seconds in (**F**). (**G**, **H**) The response topographies for 445 nm at 35.0 seconds shown in (**F**) and (**H**) measured in the perimacular region in (**G**). The color scale indicates the relative reflectance changes (%) at 35.0 minutes to the reflectance at 12.5 minutes. Data from Monkeys 2 and 1 are presented for rod and S-cone, respectively.

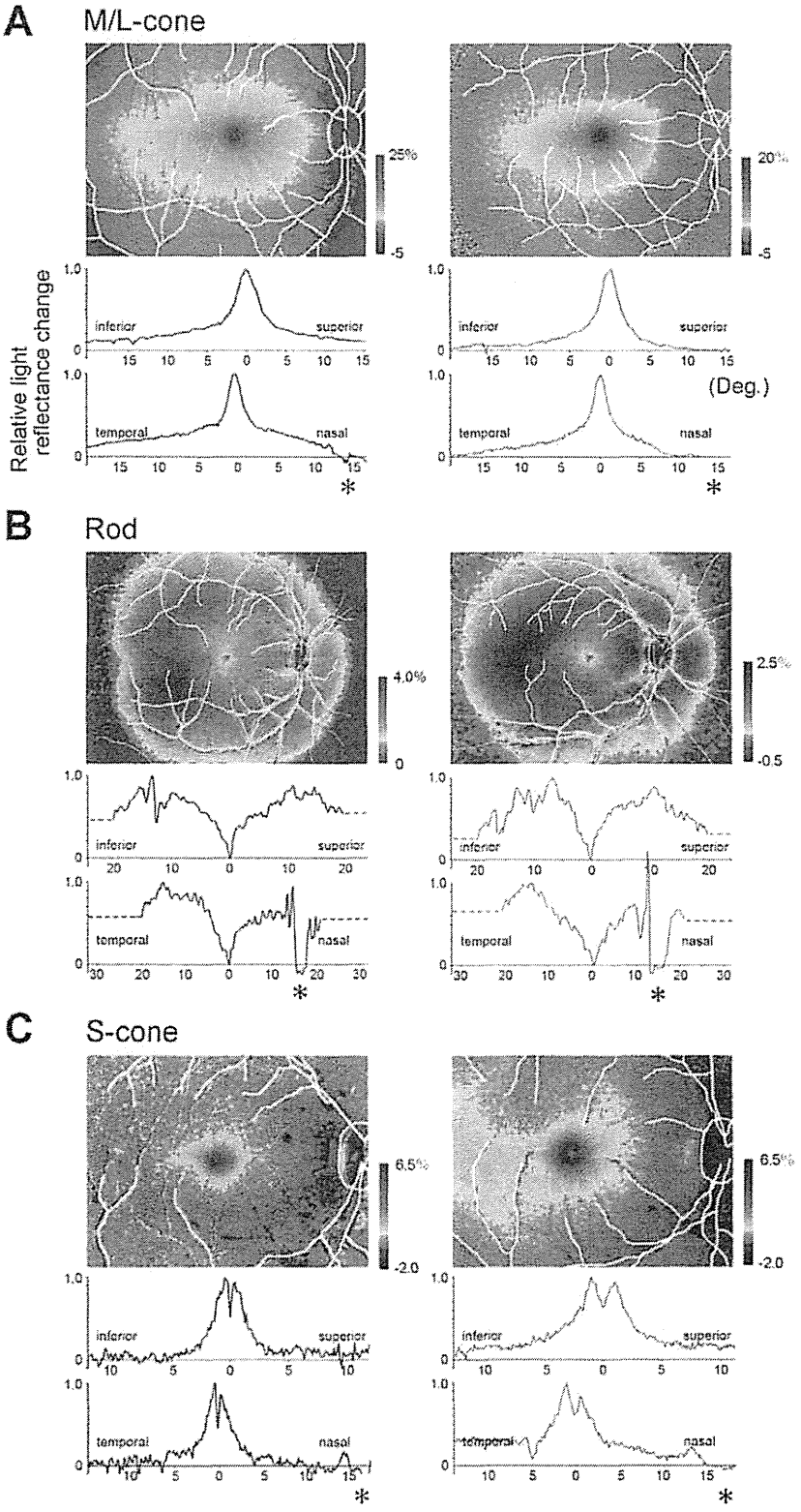

FIGURE 3. Pseudo-color functional topographies for the three types of photoreceptors in two monkeys. (A–C) pseudo-colored functional topographic maps for the three types of photoreceptors (*upper*) and relative response values to the peak (1.0) in the vertical and horizontal profile along the foveal center (*lower*). (A) Response topographies for the M/L cones obtained by 5.35 log phot. td between 60 to 180 seconds following the illumination. (B) Response topographies for the rods obtained by 4.73 log scot. tld between 52.5 to 150 seconds following the illumination. The response profiles outside the region of interest are shown as dotted lines. (C) Response topographies for the S-cone, obtained by 4.58 log phot. td between 30 to 60 seconds following the illumination. Locations of the retinal vessels are overlaid by white lines. Zero degree in the response profile

pattern with an annular peak at an eccentricity of 9.4 to 14.0 degrees from the fovea (Fig. 2D).

The light reflectance changes with 445 nm of 4.58 log phot. td during the initial 75 seconds are expanded in Figure 2E. The time-course at the temporal retina was flatter 12.5 seconds after the onset of bleaching (Fig. 2E, blue line). The reflectance changes relative to the reflectance value at 12.5 seconds after the onset (arrowhead in Fig. 2E) are re-plotted in Figure 2F. During the initial 22.5 seconds (underlined by gray), the degree of reflectance increased to 13.7% at the fovea (red line), but remained flat at the temporal retina (blue line). The light reflectance at the peripheral region did not increase during this period due to the conversion from Meta-II intermediates (peak 380 nm) to Meta-III intermediates (peak 465 nm) of the rod photopigments.[36,37] These changes indicated that the topography obtained during this period did not reflect the responses of rods but was dominated by S-cones. Thus, the topography of S-cone bleaching in the macula could be obtained, and it had a volcano-shaped activation with the foveal center largely excavated (Fig. 2H). This is considered to reflect the reduced number of S-cones at the fovea.

Functional Topography of M/L Cones, Rods, and S-Cones

By considering the preferred wavelengths and the characteristic time courses of the reflectance changes, we have shown the functional topographies of the M/L-cones, rods and S-cones in two monkeys (Fig. 3) in horizontal and vertical sections. The distribution of M/L-cones response had a steep peak at the foveal center and was elongated horizontally. The distribution of rod responses was minimum at the foveal center and maximum along the circular region at the eccentricity of the optic disc. The distribution of S-cone responses was highest at the fovea and was excavated centrally. There was a circular region with the maximal responses at 0.38 to 1.0 degrees from the foveal center.

Discussion

We determined the functional topographic maps of rods, M/L-cones, and S-cones based on the differences in retinal reflectance changes after a selective bleaching of the photopigments by using a flood illumination camera system. A confocal SLO system also could have been used because it has the better spatial resolution. In addition, the intensity of illumination falling on the retina can be homogeneous and modifications of the optical pathway would not be needed as with the fundus camera. However, the most important part of this study was not the imaging resolution alone, but the ability to obtain functional topographic maps of different types of photoreceptors by using different combinations of wavelengths, stimulus intensities, and stimulus durations (Fig. 2). These combinations allowed us to segregate the responses of the different types of photoreceptors. We conducted preliminary experiments with various band pass interference filters and concluded that the combination of 445, 500, and 590 nm filters was ideal for our purposes. In that sense, the simplicity of a flood illumination camera system was advantageous for us.

In the M/L cones (Fig. 3A), the reflectance pattern was approximately equal to that obtained by anatomical studies in macaque and human retinas.[3,4] The reflectance distribution was elongated horizontally with a peak at the foveal center.

In the rods (Fig. 3B), the reflectance changes were minimal at the foveal center, and increased rapidly toward the periphery. The reflectance distribution had a "rod ring" at the eccentricity of the optic disc, that is 9.4 to 14.0 degrees from the center as has been detected by anatomical studies.[3,4] The vertical gradient toward the superior retina described by Curcio et al.[3,4] could not be observed, but instead, the rod responses were maximum at the temporal region along the rod ring.

In the S-cones (Fig. 3C), the reflectance distribution had a volcano-like excavation at the foveal center. The S-cone-free region at the foveal center has been found in macaques and humans anatomically[2,5,7] and psychophysically.[11,13,38] Our results showed that S-cones are functionally minimal at the foveal center in the macaques. The diameter of the ring-shaped peaks with maximal reflectance changes was 0.83 degrees (vertically) x 0.75 degrees (horizontally) in M1 and 1.99 × 1.55 degrees in M2 (Fig. 1C). The eccentricities of the S-cone peaks were within the variations of those obtained by anatomical[2,5,7] and psychophysical studies.[11,13,38] The locations of the peaks of the S-cone responses varied among individuals and the ring-shaped peaks looked vertically elongated. We should note that the reflectance topography of S-cones was shown reliably only in the macular region because the S-cone activities in the periphery were relatively small[12] and were cancelled by the rod-induced light reflectance changes (Fig. 2E and 2F).

There are some discrepancies between the results of earlier anatomical studies and our imaging results. This is because the densitometry technique does not depend solely on the density of photoreceptors, but also on the length of photoreceptor outer segments, that is density of photopigments in each photoreceptor. The goal of our study, however, was not to map the density of the photoreceptors, which has been done already through the series of studies by Curcio et al.,[3–5] but to draw the activity-dependent topography of the photoreceptors, which may confirm and augment the response topography obtained by, for example, mutifocal ERGs.

In our technique of fundus reflectometry, the optical pathway was adjusted to illuminate the posterior retina homogeneously so that the results reflected the relative reflectance distribution more accurately. However, there are some possible artifacts by which the reflectance changes may be either over- or underestimated in particular regions. First, the presence of scattered light from the inner limiting membrane and nerve fiber layer around the macula may cause an underestimation of the bleach-induced light reflectance changes.[31] A quantitative evaluation of this scattering effect was very difficult to obtain because the topographies we had presented did not seem to be affected by such artifacts in the peri-macular regions (Fig. 3A).

Second, the effect of intrinsic optical signals, which reflect the hemoglobin-induced light reflectance changes following neural activation, must be considered.[39,40] The intrinsic signals also would be observed in the retina as stimulus-induced light reflectance decreases.[41–43] The intrinsic signals are prominent at a wavelength with the maximum hemoglobin absorption (540–580 nm), and in our response topographies, regions corresponding to the optic disc and large retinal vessels, which are rich in red blood cells, might have had relatively smaller reflectance increases due to the intrinsic signals (Figs. 1 and 3). The maximal light reflectance decrease due to intrinsic signals

indicates the location of fovea. The location of the optic disk is indicated by an asterisk. Data from Monkeys 1 and 3 for M/L cone, Monkeys 2 and 3 for rods, and Monkeys 1 and 2 for S-cones are presented.

in our recording protocol, however was estimated to be 1.0% to 2.0% at the optic disc, where intrinsic signals could be solely and maximally observed.[42] Thus, the intrinsic signals probably had little effect on the overall bleaching topographies.

Third, the Stiles-Crawford effect,[44] the directional sensitivity of the cone photoreceptors, may change the reflectance intensities depending on the position of the illumination center over the retina. In the horizontal response profiles of S-cones (Fig. 3C), the circular peak response was slightly higher in the temporal fovea than in the nasal fovea. This was considered to reflect the Stiles-Crawford effect because the illumination was centered 2.56 degrees temporal to the foveal center, and the rays of light passed cone photoreceptors less oblique at the temporal fovea than at the nasal fovea.

The bleach-induced reflectance changes are affected by such artifacts and may not reflect the distribution of photoreceptor activities accurately.

A clinical application of this technique may not be easy because subjects must keep staring at the fixation target with very bright background illumination for relatively long times. However, there are recent reports using SLO[31,45,46] or a snapshot imaging system[33] to measure cone- or rod-induced response topography. Unfortunately, the response distribution of rods or S-cone responses cannot be extracted accurately as in this study. Our results will provide us with valuable photoreceptor activities in macaque retinas, which can complement those obtained either anatomically[2–5,7] or psychophysically.[10–15,38]

References

1. Osterberg G. Topography of the layer of rods and cones in the human retina. *Acta Ophthalmol.* 1935;13:6–97.
2. de Monasterio FM, McCrane EP, Newlander JK, Schein SJ. Density profile of blue-sensitive cones along the horizontal meridian of macaque retina. *Invest Ophthalmol Vis Sci.* 1985; 26:289–302.
3. Packer O, Hendrickson AE, Curcio CA. Photoreceptor topography of the retina in the adult pigtail macaque (Macaca nemestrina). *J Comp Neurol.* 1989;288:165–183.
4. Curcio CA, Sloan KR, Kalina RE, Hendrickson AE. Human photoreceptor topography. *J Comp Neurol.* 1990;292:497–523.
5. Curcio CA, Allen KA, Sloan KR, et al. Distribution and morphology of human cone photoreceptors stained with anti-blue opsin. *J Comp Neurol.* 1991;312:610–624.
6. Mollon JD, Bowmaker JK. The spatial arrangement of cones in the primate fovea. *Nature.* 1992;360:677–679.
7. Bumsted K, Hendrickson A. Distribution and development of short-wavelength cones differ between Macaca monkey and human fovea. *J Comp Neurol.* 1999;403:502–516.
8. Andrade da Costa BL, Hokoc JN. Photoreceptor topography of the retina in the New World monkey Cebus apella. *Vision Res.* 2000;40:2395–2409.
9. Cornish EE, Hendrickson AE, Provis JM. Distribution of short-wavelength-sensitive cones in human fetal and postnatal retina: early development of spatial order and density profiles. *Vision Res.* 2004;44:2019–2026.
10. Wald G. The receptors of human color vision. *Science.* 1964; 145:1007–1016.
11. Wald G. Blue-blindness in the normal fovea. *J Opt Soc Am.* 1967;57:1289–1301.
12. Wooten BR, Wald G. Color-vision mechanisms in the peripheral retinas of normal and dichromatic observers. *J Gen Physiol.* 1973;61:125–145.
13. Castaño JA, Sperling HG. Sensitivity of the blue-sensitive cones across the central retina. *Vision Res.* 1982;22:661–673.
14. Birch DG, Herman WK, deFaller JM, Disbrow DT, Birch EE. The relationship between rod perimetric thresholds and full-field rod ERGs in retinitis pigmentosa. *Invest Ophthalmol Vis Sci.* 1987;28:954–965.
15. Pulos E. Changes in rod sensitivity through adulthood. *Invest Ophthalmol Vis Sci.* 1989;30:1738–1742.
16. Rushton WA. The rhodopsin density in the human rods. *J Physiol.* 1956;134:30–46.
17. Hood C, Rushton WA. The Florida retinal densitometer. *J Physiol.* 1971;217:213–229.
18. Brown PK, Wald G. Visual pigments in human and monkey retinas. *Nature.* 1963;200:37–43.
19. Rushton WA. Cone pigment kinetics in the protanope. *J Physiol.* 1963;168:374–388.
20. Brown PK, Wald G. Visual pigments in single rods and cones of the human retina. direct measurements reveal mechanisms of human night and color vision. *Science.* 1964;144:45–52.
21. Alpern M, Maaseidvaag F, Oba N. The kinetics of cone visual pigments in man. *Vision Res.* 19771;11:539–549.
22. Alpern M. Rhodopsin kinetics in the human eye. *J Physiol.* 1971;217:447–471.
23. Mizuno K, Majima A, Ozawa K, Ito H. Red-free light fundus photography. Photographic optogram. *Invest Ophthalmol.* 1968;7:241–249.
24. Highman VN, Weale RA. Rhodopsin density and visual threshold in retinitis pigmentosa. *Am J Ophthalmol.* 1973; 75:822–832.
25. Sheorey UB. Clinical assessment of rhodopsin in the eye. Using a standard fundus camera and a photographic technique. *Br J Ophthalmol.* 1976;60:135–141.
26. Kilbride PE, Read JS, Fishman GA, Fishman M. Determination of human cone pigment density difference spectra in spatially resolved regions of the fovea. *Vision Res.* 1983;23:1341–1350.
27. Kilbride PE, Keehan KM. Visual pigments in the human macula assessed by imaging fundus reflectometry. *Appl Opt.* 1990;29: 1427–1435.
28. Faulkner DJ, Kemp CM. Human rhodopsin measurement using a T.V.-based imaging fundus reflectometer. *Vision Res.* 1984; 24:221–231.
29. Kemp CM, Faulkner DJ, Jacobson SG. The distribution and kinetics of visual pigments in the cat retina. *Invest Ophthalmol Vis Sci.* 1988;29:1056–1065.
30. van Norren D, van de Kraats J. Imaging retinal densitometry with a confocal Scanning Laser Ophthalmoscope. *Vision Res.* 1989;29:1825–1830.
31. Elsner AE, Burns SA, Hughes GW, Webb RH. Reflectometry with a scanning laser ophthalmoscope. *Appl Opt.* 1992;31: 3697–3710.
32. Berendschot TT, DeLint PJ, van Norren D. Fundus reflectance-historical and present ideas. *Prog Retin Eye Res.* 2003;22:171–200.
33. Kazato Y, Shibata N, Hanazono G, Suzuki W, Tanifuji M, Tsunoda K. Novel snapshot imaging of photoreceptor bleaching in macaque and human retinas. *Jpn J Ophthalmol.* 2010;54:349–356.
34. Bowmaker JK, Dartnall HJ. Visual pigments of rods and cones in a human retina. *J Physiol.* 1980;298:501–511.
35. Bowmaker JK, Dartnall HJ, Mollon JD. Microspectrophotometric demonstration of four classes of photoreceptor in an old world primate, Macaca fascicularis. *J Physiol.* 1980;298:131–143.
36. Imai H, Kuwayama S, Onishi A, Morizumi T, Chisaka O, Shichida Y. Molecular properties of rod and cone visual pigments from purified chicken cone pigments to mouse rhodopsin in situ. *Photochem Photobiol Sci.* 2005;4:667–674.

37. Shichida Y, Imai H, Imamoto Y, Fukada Y, Yoshizawa T. Is chicken green-sensitive cone visual pigment a rhodopsin-like pigment - a comparative-study of the molecular-properties between chicken green and rhodopsin. *Biochemistry*. 1994; 33:9040-9044.
38. Williams DR, MacLeod DI, Hayhoe MM. Punctate sensitivity of the blue-sensitive mechanism. *Vision Res*. 1981;21:1357-1375.
39. Grinvald A, Lieke E, Frostig RD, Gilbert CD, Wiesel TN. Functional architecture of cortex revealed by optical imaging of intrinsic signals. *Nature*. 1986;324:361-364.
40. Bonhoeffer T, Grinvald A. Optical imaging based on intrinsic singals: the methodology. In: Toga AW, Mazziotta JC, eds. *Brain Mapping*. San Diego: Academic Press; 1996:55-97.
41. Tsunoda K, Oguchi Y, Hanazono G, Tanifuji M. Mapping cone- and rod-induced retinal responsiveness in macaque retina by optical imaging. *Invest Ophthalmol Vis Sci*. 2004;45:3820-3826.
42. Hanazono G, Tsunoda K, Kazato Y, Tsubota K, Tanifuji M. Evaluating neural activity of retinal ganglion cells by flash-evoked intrinsic signal imaging in macaque retina. *Invest Ophthalmol Vis Sci*. 2008;49:4655-4663.
43. Tsunoda K, Hanazono G, Inomata K, Kazato Y, Suzuki W, Tanifuji M. Origins of retinal intrinsic signals: a series of experiments on retinas of macaque monkeys. *Jpn J Ophthalmol*. 2009;53:297-314.
44. Stiles WS, Crawford BH. The luminous efficiency of rays entering the eye pupil at different points. *Proc Roy Soc London Series B-Containing Papers of a Biological Character*. 1933;112:428-450.
45. Elsner AE, Burns SA, Beausencourt E, Weiter JJ. Foveal cone photopigment distribution: small alterations associated with macular pigment distribution. *Invest Ophthalmol Vis Sci*. 1998;39:2394-2404.
46. Sekiryu T, Iida T, Maruko I, Horiguchi M. Clinical application of autofluorescence densitometry with a scanning laser ophthalmoscope. *Invest Ophthalmol Vis Sci*. 2009;50:2994-3002.

A Longitudinal Study of Stargardt Disease: Clinical and Electrophysiologic Assessment, Progression, and Genotype Correlations

KAORU FUJINAMI, NOEMI LOIS, ALICE E. DAVIDSON, DONNA S. MACKAY, CHRIS R. HOGG, EDWIN M. STONE, KAZUSHIGE TSUNODA, KAZUO TSUBOTA, CATEY BUNCE, ANTHONY G. ROBSON, ANTHONY T. MOORE, ANDREW R. WEBSTER, GRAHAM E. HOLDER, AND MICHEL MICHAELIDES

• PURPOSE: To investigate the clinical and electrophysiologic natural history of Stargardt disease and correlate with the genotype.

• DESIGN: Cohort study of 59 patients.

• METHODS: Clinical history, examination, and electrophysiologic assessment were undertaken in a longitudinal survey. Patients were classified into 3 groups based on electrophysiologic findings, as previously published: Group 1 had dysfunction confined to the macula; Group 2 had macular and generalized cone system dysfunction; and Group 3 had macular and both generalized cone and rod system dysfunction. At baseline, there were 27 patients in Group 1, 17 in Group 2, and 15 in Group 3. Amplitude reduction of >50% in the relevant electroretinogram (ERG) component or a peak time shift of >3 ms for the 30 Hz flicker ERG or bright flash a-wave was considered clinically significant ERG deterioration. Molecular screening of *ABCA4* was undertaken.

• RESULTS: The mean age at baseline was 31.7 years, with the mean follow-up interval being 10.5 years. A total of 22% of patients from Group 1 showed ERG group transition during follow-up, with 11% progressing to Group 2 and 11% to Group 3. Forty-seven percent of patients in Group 2 progressed to Group 3. There was clinically significant ERG deterioration in 54% of all subjects: 22% of Group 1, 65% of Group 2, and 100% of Group 3. At least 1 disease-causing *ABCA4* variant was identified in 47 patients.

• CONCLUSIONS: All patients with initial rod ERG involvement demonstrated clinically significant electrophysiologic deterioration; only 20% of patients with normal full-field ERGs at baseline showed clinically significant progression. Such data assist counseling by providing more accurate prognostic information and are also highly relevant in the design, patient selection, and monitoring of potential therapeutic interventions. (Am J Ophthalmol 2013;■:■–■. © 2013 by Elsevier Inc. All rights reserved.)

STARGARDT DISEASE IS ONE OF THE MOST COMMON inherited retinal disorders, with a prevalence of 1 in 10 000. It is inherited as an autosomal recessive trait.[1–3] Most cases present with central visual loss and there is typically macular atrophy with yellow-white flecks at the posterior pole, which are at the level of the retinal pigment epithelium (RPE). Autofluorescence (AF) imaging and fluorescein angiography can be helpful in confirming the diagnosis.[4–8] The age of onset is usually in the early teens, but there is wide variation, with a later age of onset being associated with a better visual prognosis.[7,9]

Since the discovery of *ABCA4* variants underlying Stargardt disease, multiple studies have described the wide phenotypic variability in *ABCA4*-associated retinopathy.[9–19] There is also extensive allelic heterogeneity, with more than 600 sequence variations having been reported to date in the *ABCA4* gene.[10,13,20–30] These 2 features make comprehensive genotype/phenotype correlations challenging. A previous cross-sectional study of 63 patients with Stargardt disease classified subjects into 3 functional electroretinogram (ERG) phenotypes: Group 1: dysfunction confined to the macula; Group 2: macular and generalized cone ERG abnormalities; and Group 3: macular and both generalized cone and rod ERG abnormalities.[31] Differences in rod or cone function between groups could not be explained by differences in age of onset or duration of disease. It was thereby concluded that these 3 groups may represent distinct phenotypic subtypes of Stargardt disease and it was suggested, based on the cross-sectional data, that patients in Group 1 were likely to have a more favorable prognosis.

AJO.com Supplemental Material available at AJO.com.

Accepted for publication Jan 16, 2013.

From the University College London, Institute of Ophthalmology, London, United Kingdom (K.F., N.L., A.E.D., D.S.M., C.R.H., A.G.R., A.T.M., A.R.W., G.E.H., M.M.); Moorfields Eye Hospital, City Road, London, United Kingdom (K.F., D.S.M., C.R.H., C.B., A.G.R., A.T.M., A.R.W., G.E.H., M.M.); Laboratory of Visual Physiology, National Institute of Sensory Organs, National Tokyo Medical Center, Tokyo, Japan (K.F., K.Tsunoda); Department of Ophthalmology, Institute of Medical Sciences, University of Aberdeen, Aberdeen, United Kingdom (N.L.); University of Iowa Institute for Vision Research, Howard Hughes Medical Institute, Iowa City, Iowa (E.M.S.); and Department of Ophthalmology, Keio University School of Medicine, Tokyo, Japan (K.Tsubota).

Inquiries to Mr Michel Michaelides, University College London, Institute of Ophthalmology, 11-43 Bath St, London EC1V 9EL, United Kingdom; e-mail: michel.michaelides@ucl.ac.uk

0002-9394/$36.00
http://dx.doi.org/10.1016/j.ajo.2013.01.018

The purpose of the present study was to determine whether longitudinal data from a cohort of Stargardt disease patients support the value of full-field ERG to visual prognosis previously suggested by cross-sectional data. We have assessed the progression of Stargardt disease by repeated clinical and electrophysiologic examinations over time and probed whether the initial phenotype predicts long-rerm prognosis.

PATIENTS AND METHODS

A COHORT OF 59 PATIENTS WITH A CLINICAL DIAGNOSIS OF Stargardt disease and a minimum of 7 years of follow-up were ascertained at Moorfields Eye Hospital. All patients were first diagnosed between 1997 and 2000, with the latest examinations performed between 2009 and 2011. The baseline clinical and electrophysiologic characteristics of 33 of these 59 patients have been previously reported.[31] The panel included 5 sibships (4 sibling pairs and 1 set of 3 siblings). Informed consent was obtained from all participants. Blood samples were taken from all individuals for DNA extraction. The protocol of the study adhered to the tenets of the Declaration of Helsinki and was approved by the Ethics Committee of Moorfields Eye Hospital.

• CLINICAL ASSESSMENT: Fifty-nine patients were assessed on at least 2 occasions, with the first and most recent visits taken as the baseline and "follow-up" examinations, respectively, for the purposes of data analysis. A full medical history was obtained and a comprehensive ophthalmologic examination performed for all patients. The age of onset was defined as the age at which visual loss was first noted by the patient. The duration of the disease was calculated as the difference between age at onset and age at the baseline examination when an electrophysiologic assessment was obtained. The inrerval of observation was determined by the difference between the age at baseline and the age at the most recent electrophysiologic examination. Clinical assessment included best-corrected Snellen visual acuity (converted to equivalent logarithm of minimal angle of resolution [logMAR] visual acuity for the purpose of data analysis), dilated ophthalmoscopy, and color fundus photography.

• ELECTROPHYSIOLOGY: All patients underwent electrophysiologic assessment, to include full-field ERG and pattern electroretinography (PERG), incorporating the minimum standards of the International Society for Clinical Electrophysiology of Vision (ISCEV).[32,33] ERG examination was comprehensive and included: (1) dark-adapted dim flash 0.01 candela second (cd·s)/m^2 (dark-adapted 0.01); (2) dark-adapted bright flash 11.0 cd·s/m^2 (dark-adapted 11.0); (3) light-adapted 3.0 cd·s/m^2 30 Hz flicker ERG (light-adapted 30 Hz); and (4) light-adapted 3.0 cd·s/m^2 at 2 Hz (light-adapted 3.0). All recordings were performed with gold-foil recording electrodes with reference electrodes at the ipsilateral outer canthi.

The patient data were compared against those of 16 healthy subjects younger than 50 years and 19 subjects older than 50 years, to maintain consistency with the original cross-sectional study.[4,31,34] PERGs were compared against those from 28 normal subjects, with N95 peak time not being used for interpretation because of its accepted variability.[35] The limits of ERG normality were defined for all the components of the ERG and PERG as the mean value ±2 standard deviations (Supplemental Tables 1 and 2, available at AJO.com). The threshold values for the minimum amplitude/maximum peak time for subjects younger than 50 years were defined as 135 μV/107 ms (dark-adapted 0.01), 250 μV/13 ms and 320 μV/56 ms (dark-adapted 11.0 a- and b-wave, respectively), 70 μV/27 ms (light-adapted 30 Hz), and 30 μV/15 ms and 95 μV/32 ms (light-adapted 3.0 a- and b-wave, respectively); and for patients older than 50 years as 30 μV/117 ms (dark-adapted 0.01), 105 μV/16 ms and 235 μV/57 ms (dark-adapted 11.0 a- and b-wave, respectively), 50 μV/29 ms (light-adapted 30 Hz); and 15 μV/16 ms and 90 μV/32 ms (light-adapted 3.0 a- and b-wave, respectively). The threshold values for the PERG P50 minimum amplitude/maximum peak time were defined as 2.1 μV/58.5 ms.

All the components of the ERG and PERG from each eye were taken into account when classifying patients into 1 of the 3 ERG groups at baseline and follow-up. Group 1 was defined as PERG abnormality with normal ERGs. In Group 2, there was PERG abnormality and abnormal cone function (assessed with light-adapted 30 Hz and light-adapted 3.0) on ERG. In Group 3, there was additional rod ERG abnormality (assessed using dark-adapted 0.01 and dark-adapted 11.0). The overall classification was based on the more severe eye in the small number of patients with different ERG groups between eyes. The data obtained at follow-up were compared with those at baseline. Concordance for ERG group between siblings was defined as siblings having the same ERG group classification both at baseline and at follow-up.

Amplitude reduction was calculated as the difference between amplitude at baseline and at follow-up. The percentage reduction in amplitudes was obtained by dividing the amplitude reduction by baseline amplitude. A yearly amplitude reduction and a yearly percentage reduction were calculated by dividing the amplitude reduction or the percentage reduction by the follow-up time. A yearly peak time shift (difference between peak time at baseline and at follow-up) was also calculated by dividing by the follow-up time.

An amplitude reduction of over 50% in any ERG component and/or a peak time shift of over 3 ms for the light-adapted 30 Hz ERG or dark-adapted 11.0 ERG a-wave were considered evidence of clinically significant ERG deterioration/progression. Patients were thereby

classified into 2 subsets: those with clinically significant ERG deterioration and those without significant ERG deterioration (stable ERG).

• MUTATION SCREENING: Mutation analysis was performed using the single-stranded conformation polymorphism (SSCP) strategy of the whole coding region of *ABCA4* in 33 subjects[36] and the arrayed primer extension (APEX) microarray (ABCR400 chip; Asper Ophthalmics, Tartu, Estonia) for previously reported variants in 27 patients.[23] Direct Sanger sequencing was done in siblings of probands and parents, when available, to confirm segregation of alleles, as well as in 8 subjects either to confirm putative novel variants or where the variants found with SSCP and APEX differed (Supplemental Table 3, available at AJO.com).

Non-null variants were analyzed using 2 software prediction programs: SIFT (Sorting Intolerant from Tolerant; http://sift.jcvi.org/)[37] and PolyPhen2 (http://genetics.bwh.harvard.edu/pph/index.html).[38] All variants were also analyzed for their effect on splicing using the Human Splicing Finder program, version 2.4.1 (http://www.umd.be/HSF/). All variants were compared with variants in the Exome Variant Server, NHLBI Exome Sequencing Project, Seattle, Washington, USA (http://snp.gs.washington.edu/EVS/).

Each patient was classified into 4 mutually exclusive genotype groups on the basis of the molecular analysis: (A) patients with at least 1 null variant, (B) subjects with 2 or more non-null variants, (C) individuals with 1 non-null variant, and (D) patients with no detectable variants. Null variants were those that would be expected to affect splicing, or to introduce a premature truncating codon in the protein if translated. The term "variants" for the purpose of this study includes those sequence changes previously shown to be enriched in Stargardt patients from prior studies, or for very rare variants, those not found at an allele frequency greater than 0.1% on the exome variant database (Accessed March 1, 2012).

• STATISTICAL ANALYSIS: Statistical analysis has been undertaken using data from only 1 eye in each subject. For the 57 patients with the same ERG grouping in both eyes, the eye used for analysis was selected according to the Random Integer Generator (http://www.random.org/). For the 2 patients (Patients 26 and 48) with a different ERG group in each eye, the eye with the more severe ERG grouping (ie, more generalized retinal dysfunction) was selected for analysis.

The Mann-Whitney *U* test was used to explore whether differences observed between patients with clinically significant electrophysiologic deterioration and those without were statistically significant with regard to age of onset, duration of disease, age at baseline, the interval of observation, logMAR visual acuity at baseline, logMAR visual acuity reduction (defined as the difference between visual acuity at baseline and at follow-up), and yearly percentage amplitude reduction and yearly peak time shift in both the light-adapted 11.0 a-wave and light-adapted 30 Hz.

The Kruskal-Wallis test with Steel-Dwass multiple comparisons was performed to compare the 3 baseline ERG groups (ERG Group 1, 2, and 3) and the 3 genotype groups (genotype A, B, and C) for the 10 aforementioned parameters. Where evidence was found of a difference between these groups, all pairwise comparisons were made.

The association between genotype group classification and baseline ERG group classification was tested using the Goodman-Kruskal gamma, a measure of association for ordered categories ranging between −1 and +1 for perfect negative or positive association, respectively. *P* values less than .05 were considered to indicate statistical significance.

All analyses were conducted using MedCalc statistical software version 9.2.1.0 (MedCalc Software, Ostend, Belgium) and Excel Tokei 2010 (Social Survey Research Information Co Ltd, Tokyo, Japan).

RESULTS

• CLINICAL FINDINGS: Fifty-nine patients, 31 female (52%, 31/59) and 28 male (48%, 28/59), were included in the study. All complained of central visual loss with a median age of onset of 20.8 years (range, 5-48 years) and a median duration of disease of 10.9 years (range, 0-31 years). The median ages at baseline and at follow-up were 31.7 and 42.2 years (range, 8-64 and 20-73 years), respectively. The mean follow-up interval was 10.5 years (range, 7-13 years). Seven patients (12%, 7/59) presented before 16 years of age and 52 (88%, 52/59) presented after age 16 years. The median logMAR visual acuities (VA) at baseline and at follow-up were 0.93 (range, 0.0-2.0) and 1.22 (range, 0.0-3.0), respectively, with a median logMAR VA reduction during the follow-up interval of 0.29 (range, −0.78-2.0). The clinical findings are summarized in Table 1 and the eye selected for data analysis is shown in Supplemental Table 3 (available at AJO.com).

At baseline, there were 27 patients (46%, 27/59) in Group 1, 17 (29%, 17/59) in Group 2, and 15 (25%, 15/59) in Group 3, compared at follow-up to 21 patients (36%, 21/59) in Group 1, 12 (20%, 12/59) in Group 2, and 26 (44%, 26/59) in Group 3 (Table 2). The median age of onset for each baseline ERG group was 24.9 years in Group 1, 20.4 years in Group 2, and 14.0 years in Group 3. The median age (years) at examination/logMAR visual acuity at baseline and follow-up for each baseline ERG group was 34.4/0.78 and 45.0/1.00, respectively, in Group 1; 29.6/1.00 and 39.4/1.00, respectively, in Group 2; and 29.1/1.25 and 40.3/1.30, respectively, in Group 3 (Table 3).

Color fundus photographs of eyes in 3 representative cases (Patients 17, 42, and 53) are shown in Figure 1; their

TABLE 1. Clinical Data and Molecular Genetic Status of 59 Patients With Stargardt Disease

Pt	Onset (y)	Age (y)		logMAR VA		Variants Identified[a]
		BL	FU	BL	FU	
1	16	17	26	0.0/1.0	0.0/0.48	c.768G>T / p.Gly863Ala / p.Arg943Gln
2	15	17	25	0.78/0.78	1.0/1.0	p. Arg1443His
3	11	18	27	0.78/1.0	1.0/1.0	**p.Trp439*** / p.Gly863Ala / p.Leu1970Phe
4	19	21	32	0.78/0.78	1.0/1.0	p.Leu2027Phe
5	10	22	30	0.48/0.48	1.0/0.78	p.Gly863Ala / p.Arg943Gln / c.5461-10 T>C
6	18	26	37	0.78/1.0	1.0/1.0	p.Pro1380Phe
7	25	28	40	0.78/1.0	1.3/0.78	ND
8	24	29	38	1.0/0.78	1.0/1.0	p.Phe418Ser / p.Leu2027Phe
9	24	31	44	1.0/1.0	1.3/1.0	c.4253+5 G>T / **p.Gly1507Arg**
10	26	32	44	0.78/0.78	1.0/1.0	p.Cys1490Tyr / p.Arg2030Gln
11	31	34	46	0.18/0.3	0.6/0.7	ND
12	17	35	47	1.0/1.0	1.0/1.0	p.Asn96His
13	23	35	45	1.0/0.3	1.0/0.48	p.Gly1513Profs*1554
14	33	37	48	0.18/1.48	1.0/1.3	ND
15	38	40	51	0.18/0.78	1.0/1.0	p.Arg2107His
16	42	43	53	0.0/0.0	1.0/1.0	ND
17	22	48	59	1.0/1.0	1.0/1.0	p.Cys54Tyr
18	20	49	59	1.0/0.6	1.0/1.0	p.Pro1380Leu / p.Gly1961Glu
19	35	50	61	1.0/0.3	1.0/1.0	p.Arg1108Cys
20	25	56	67	1.3/0.18	1.0/1.0	**p.Trp439*** / p.Gly863Ala
21	48	59	71	1.0/0.78	1.0/1.0	p. Ile156 Val / **p. Cys1455Arg** / **p. Phe1839Ser**
22	21	22	31	0.3/1.0	1.0/1.0	p.Arg2107His
23	21	23	33	1.0/1.0	1.0/1.0	p.Gly863Ala
24	48	64	73	0.0/1.0	0.18/3.0	p.Tyr1652*
25	17	19	29	0.78/0.3	1.0/1.0	c.5461-10 T>C
26	17	21	33	1.0/0.78	1.0/1.0	ND
27	27	53	66	1.78/1.78	1.3/1.0	p.Ser1071Cysfs*1084
28	5	14	21	0.78/0.78	1.0/1.0	p.Arg408* / **p.Val675Ile**
29	9	15	27	1.08/1.08	1.0/1.0	p.Cys2150Tyr
30	14	24	32	1.0/0.78	1.0/1.0	ND
31	18	28	39	1.0/1.0	1.0/1.0	p.Gly863Ala / p.Arg1108Cys / p.Arg943Gln
32	14	29	37	1.0/1.0	1.0/1.0	p.Arg653Cys / p.Arg2030Gln
33	19	29	40	1.0/1.0	1.0/1.08	ND
34	34	40	49	0.3/0.48	1.0/1.0	p.Gly863Ala / p.Glu1087Lys
35	25	43	54	1.0/1.0	1.0/1.0	p.Cys54Tyr / p.Gly863Ala
36	38	60	69	1.0/1.0	1.3/1.08	p.Val931Met / c.5461-10 T>C
37	10	11	20	1.0/0.78	1.3/1.3	p.Pro1380Leu
38	10	15	23	1.0/1.0	1.3/1.3	p.Ser1071Cysfs*1084 / p.Pro1380Leu
39	24	25	38	1.56/0.3	2.0/2.0	c.5461-10 T>C / c.5714+5 G>A
40	18	26	36	1.3/1.3	2.0/1.3	ND
41	32	33	45	0.48/0.48	1.0/1.0	ND
42	32	35	46	1.3/0.0	3.0/1.0	p.Cys54Tyr
43	30	35	45	0.48/0.48	2.0/1.3	ND
44	15	41	49	1.3/1.3	2.0/1.3	p.Asn965Ser
45	8	8	20	0.78/0.78	1.0/1.0	p.Thr1019Met
46	10	11	23	1.0/1.0	1.0/1.0	p.Thr1019Met
47	8	12	24	2.0/1.56	1.78/1.48	p.Cys2150Tyr
48	17	18	26	1.0/0.78	1.3/1.0	c.5461-10 T>C / p.Leu2027Phe
49	8	21	33	1.3/1.3	2.0/2.0	p.Asp574Aspfs*582
50	8	27	39	2.0/1.56	1.78/1.48	c.5461-10 T>C
51	24	31	43	1.18/1.18	1.08/1.3	p.Arg1640Trp / p.Leu2027Phe

Continued on next page

TABLE 1. Clinical Data and Molecular Genetic Status of 59 Patients With Stargardt Disease (*Continued*)

Pt	Onset (y)	Age (y)		logMAR VA		Variants Identified[a]
		BL	FU	BL	FU	
52	11	31	42	1.3/1.3	2.0/2.0	p.Arg1108His
53	5	32	43	2.0/2.0	2.0/2.0	c.5461-10 T>C / p.Cys2150Tyr
54	5	32	43	2.0/2.0	2.0/2.0	c.5461-10 T>C / p.Cys2150Tyr
55	7	36	47	1.3/1.3	3.0/1.3	c.5461-10 T>C / p.Cys2150Tyr
56	13	39	50	1.25/1.56	3.0/3.0	ND
57	23	42	52	1.56/1.0	1.0/1.0	p.Leu747Cysfs*787
58	40	43	54	0.18/0.18	0.78/0.78	ND
59	23	54	65	0.78/1.0	1.0/1.0	p.Ile156Val

BL = baseline; FU = follow-up; logMAR = logarithm of minimal angle of resolution; ND = not detected; Pt = patient; VA = visual acuity.
[a]Putative novel changes are shown in bold.

TABLE 2. Distribution of Electrophysiologic Groups at Baseline and at Follow-up in Stargardt Disease

Electrophysiologic Group[a] at Baseline[b]	Electrophysiologic Group[a] at Follow-up[b]		
	Group 1	Group 2	Group 3
Group 1 (n = 27, **6**)	21	3 (**3**)	3 (**3**)
Group 2 (n = 17, **11**)		9 (**3**)	8 (**8**)
Group 3 (n = 15, **15**)			15 (**15**)
Total (n = 59, **32**)	21	12 (**6**)	26 (**26**)

[a]Patients were classified into 3 groups based on electrophysiologic findings: Group 1 had dysfunction confined to the macula; Group 2 had macular and generalized cone system dysfunction; Group 3 had macular and both generalized cone and rod system dysfunction.
[b]Numbers in bold show the numbers of patients who demonstrated electrophysiologic evidence of deterioration. An amplitude reduction of over 50% in any electrophysiologic component and/or a peak time shift of over 3 ms for the light-adapted 30 Hz electroretinogram or dark-adapted 11.0 electroretinogram a-wave were considered evidence of significant electrophysiologic deterioration.

respective electrophysiologic traces appear in Figure 2. Patient 17 showed no ERG group transition (Group 1 at baseline and Group 1 at follow-up). ERG transition from Group 2 to Group 3, with clinically significant ERG deterioration, was demonstrated in Patient 42. Patient 53 was in ERG Group 3 at baseline and had evidence of clinically significant ERG deterioration.

• ELECTROPHYSIOLOGIC FINDINGS: The electrophysiologic findings are summarized in Supplemental Table 4 (available at AJO.com). PERG P50 components were undetectable (93%, 51/55) or moderately reduced (7%, 4/55; Patients 16, 24, 42, and 55) at baseline, in keeping with severe or moderately severe macular dysfunction; and were undetectable in 53 individuals (96%, 53/55) or moderately reduced in 2 patients (4%, 2/55; Patients 16 and 24) at follow-up. There were no available PERG data both at baseline and at follow-up in 2 subjects (Patients 7 and 23), and no available baseline PERGs in 2 further individuals (Patients 45 and 46), who had undetectable PERGs at follow-up.

Complete ERG data sets were available at baseline and follow-up, with few exceptions (Supplemental Table 4). The dark-adapted 0.01 and dark-adapted 11.0 ERGs were abnormal in 11 and 15 patients (20%, 11/54 and 25%, 15/59), respectively, at baseline, and in 22 and 24 subjects (36%, 22/59 and 41%, 24/59), respectively, at follow-up. All those with abnormal dark-adapted 0.01 ERGs had abnormal light-adapted 30 Hz and light-adapted 3.0 ERGs. Three out of 4 patients (Patients 53-56) with undetectable dark-adapted 0.01 responses at follow-up had undetectable light-adapted ERGs at baseline and at follow-up.

Light-adapted 30 Hz and light-adapted 3.0 ERGs were abnormal in 29 and 26 patients (49%, 29/59, and 45%, 26/58), respectively, at baseline; and in 38 and 36 subjects (64%, 38/59 and 61%, 36/59), respectively, at follow-up. An abnormal light-adapted 3.0 ERG was the only baseline ERG abnormality in 2 patients (Patients 29 and 41); isolated light-adapted 30 Hz ERG abnormality occurred in another 4 subjects (Patients 28, 30, 42, and 48). All 6 of these patients showed abnormal responses in both light-adapted tests at follow-up. Isolated light-adapted 30 Hz ERG abnormality occurred in another 2 patients at follow-up.

Four out of 5 sibships were concordant (the same ERG group) both at baseline and at follow-up (Patients 11 and 14; 40 and 42; 45 and 46; 53-55). Two siblings from 1 family had discordant ERG groups, with 1 sibling in Group 3 at baseline and follow-up and the other sibling in Group 2 at baseline and follow-up (Patients 47 and 29) (Supplemental Table 4).

The clinical features of each baseline group are summarized in Table 3 and Figure 3. There was a statistically significant difference between Groups 1 and 3 and between Groups 2 and 3 in terms of onset of disease (Supplemental Table 5, available at AJO.com). There was also

TABLE 3. *Clinical Features Associated With Electrophysiologic Group at Baseline, Electrophysiologic Deterioration, and Genotype Group in 59 Patients With Stargardt Disease*

		Median Age of Onset (y)	Median Age		Median logMAR Visual Acuity	
			BL	FL	BL	FL
Baseline electrophysiologic group	Group 1 (n = 27)	24.9	34.4	45.0	0.78	1.00
	Group 2 (n = 17)	20.4	29.6	39.4	1.00	1.00
	Group 3 (n = 15)	14.0	29.1	40.3	1.25	1.30
Evidence of clinically significant electrophysiologic deterioration[a]	Stable (n = 27)	23.4	33.5	43.8	0.78	1.00
	Significant deterioration (n = 32)	18.7	30.1	40.8	1.00	1.19
Genotype grouping[b]	Genotype A (n = 19)	17.6	32.6	42.1	1.08	1.39
	Genotype B (n = 10)	22.3	35.7	48.2	0.84	0.94
	Genotype C (n = 18)	20.0	27.8	38.4	0.90	1.20
	Genotype D (n = 12)	26.1	32.7	43.5	0.69	1.19
	Total (n = 59)	20.8	31.7	42.2	0.93	1.22

BL = baseline; FL = follow-up; logMAR = logarithm of minimal angle of resolution.

[a]The subset without evidence of significant deterioration is described as "Stable."

[b]Each patient was classified into 4 mutually exclusive genotype groups on the basis of the molecular analysis: (A) patients with at least 1 null variant, (B) subjects with 2 or more non-null variants, (C) individuals with 1 non-null variant, and (D) patients with no detectable variants.

a statistically significant difference in logMAR VA between Groups 1 and 3 and between Groups 2 and 3. No statistically significant difference was seen between groups with respect to age at baseline, duration of disease, and follow-up interval. Mean yearly electrophysiologic progression within each baseline ERG group with respect to dark-adapted 11.0 a-wave and light-adapted 30 Hz is summarized in Table 4 and Figure 3. Statistical analysis revealed a significant difference between Groups 1 and 3 and between Groups 2 and 3 in terms of yearly amplitude reduction of dark-adapted 11.0 a-wave (Supplemental Table 5). There was also a statistically significant difference in light-adapted 30 Hz yearly peak time shift between Groups 1 and 3. No significant difference was seen between groups with respect to amplitude reduction in light-adapted 30 Hz.

Thirty-two patients showed evidence of clinically significant electrophysiologic deterioration (Table 2 and Supplemental Table 4). Twenty-one subjects showed a greater than 50% amplitude reduction and 26 patients had more than a 3 ms peak time shift (Supplemental Table 4). The clinical findings were compared between the subset of patients with evidence of ERG progression and those without (stable ERG) (Table 3 and Figure 4). There was a statistically significant difference between the 2 subsets in terms of age of onset and logMAR VA at baseline (Supplemental Table 5 and Figure 4). There were no statistically significant differences between the 2 subsets with respect to age at baseline, duration of disease, interval of follow-up, and reduction in logMAR VA (Supplemental Table 5 and Figure 4).

There was clinically significant deterioration of ERG parameters in 22% (6/27) of patients in ERG Group 1, 65% (11/17) in Group 2, and 100% (15/15) in Group 3 (Table 2). Patients with a Group 1 ERG phenotype both at baseline and at follow-up did *not* show significant electrophysiologic deterioration (78%, 21/27), with the Group 1 subjects (22%, 6/27) who did show ERG progression all moving to either Group 2 or Group 3 in equal proportions. Mean yearly electrophysiologic progression was compared between patients with and without clinically significant ERG deterioration (Table 4 and Figure 4). Statistical analysis revealed a significant difference in terms of both amplitude reduction and peak time shift of dark-adapted 11.0 a-wave (Supplemental Table 5 and Figure 4). There was also a statistically significant difference in light-adapted 30 Hz peak time shift. No significant difference was seen with respect to rate of amplitude reduction in light-adapted 30 Hz (Supplemental Table 5).

• MOLECULAR GENETICS: Likely disease-causing variants in *ABCA4* were detected in 47 out of 59 patients, with 2 or more variants identified in 22 patients and 1 variant in 25 subjects (Table 1 and Supplemental Table 6, available at AJO.com). Nineteen patients had at least 1 null variant, 10 subjects had 2 or more non-null variants, 18 individuals were identified with 1 non-null variant, and 12 patients had no detectable variants. Detailed results, including *in silico* analysis to assist in the prediction of pathogenicity of the variants, are shown in Supplemental Table 7 (available at AJO.com).

Thirty-eight different variants were found in 47 patients: 11 null mutations with 3 predicted to affect splicing, and 27 non-null variants (Supplemental Tables 6 and 7). Eighteen patients harbored at least 1 null variant, with a single subject having 2 null mutations. Thirty-two of these 38 variants have been previously reported and 6 are putative novel mutations: (1) c.1317G>A, p.Trp439*, (2) c.2103G>A, p.Val675Ile, (3) c.2239delC, p.Leu747Cysfs*787, (4) c.4363C>T,

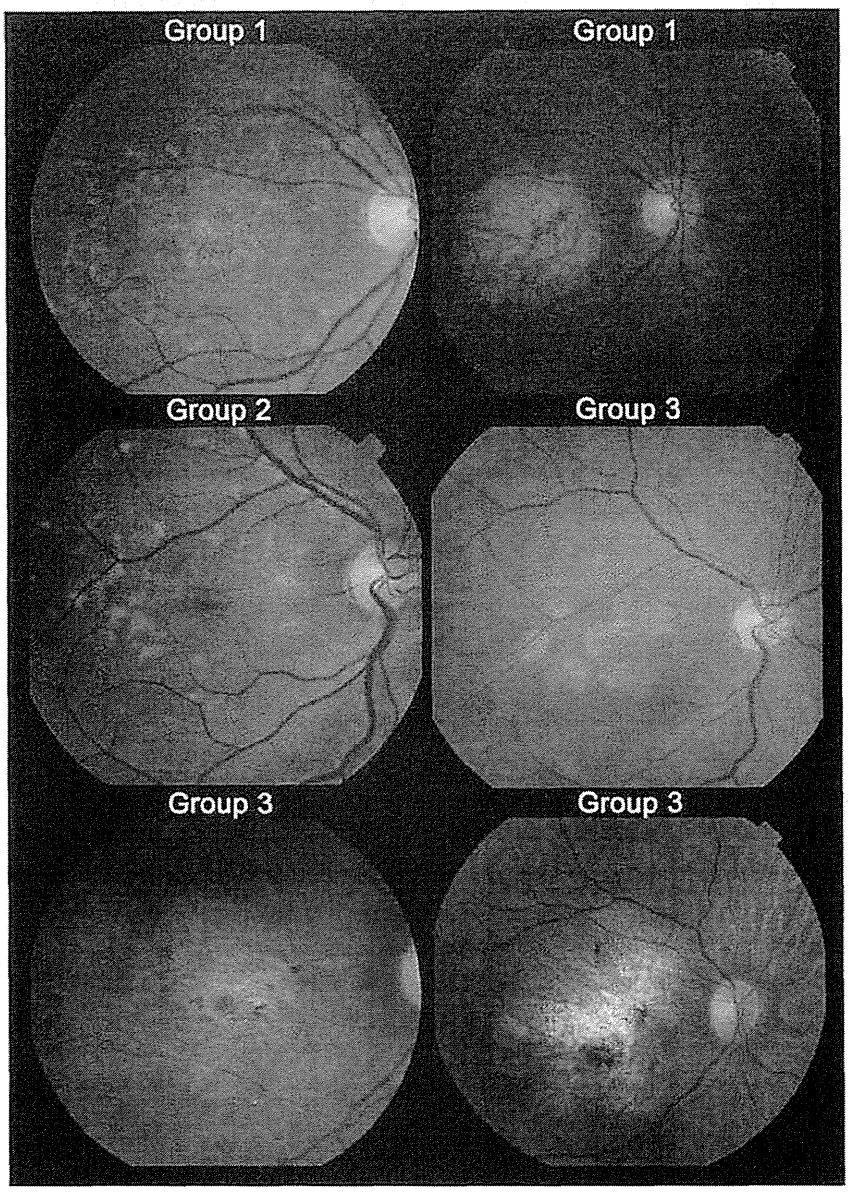

FIGURE 1. Fundus photographs of 3 representative cases of Stargardt disease (Patients 17, 42, and 53) at baseline and at follow-up depicting change over time, with the electrophysiologic group at each time point annotated. (Top) Color fundus photographs of Patient 17 showing macular atrophy surrounded by flecks at baseline (left) and severe well-defined macular atrophy surrounded by atrophic flecks at follow-up (right). Neither electrophysiologic group transition (Group 1 both at baseline and at follow-up) nor clinically significant electrophysiologic deterioration was observed in Patient 17. (Middle) Patient 42 had foveal mottling surrounded by confluent flecks at baseline (left) and multiple areas of macular atrophy at follow-up (right). Electrophysiologic transition from Group 2 to 3, with clinically significant electrophysiologic deterioration, was observed in Patient 42. (Bottom) Patient 53 had multiple areas of macular atrophy with mild pigmentation at baseline (left) and more marked macular atrophy and pigmentation at follow-up (right). Patient 53 was in Group 3 at baseline and experienced clinically significant electrophysiologic deterioration.

p.Cys1455Arg, (5) c.4519G>A, p.Gly1507Arg, and (6) c.5516T>C, p.Phe1839Ser (Supplemental Tables 6 and 7). At least 1 variant was identified in 22 patients (81%, 22/27) in ERG Group 1 at baseline, 12 (71%, 12/17) in Group 2, and 13 (87%, 13/15) in Group 3. At least 1 null variant was found in 8 patients (30%, 8/27) in ERG Group 1 at baseline, 4 (24%, 4/17) in Group 2, and 7 (47%, 7/15) in Group 3 (Supplemental Table 6 and Supplemental Figure 1, available at AJO.com).

• GENOTYPE-PHENOTYPE CORRELATIONS: Clinical features at baseline and electrophysiologic progression in dark-adapted

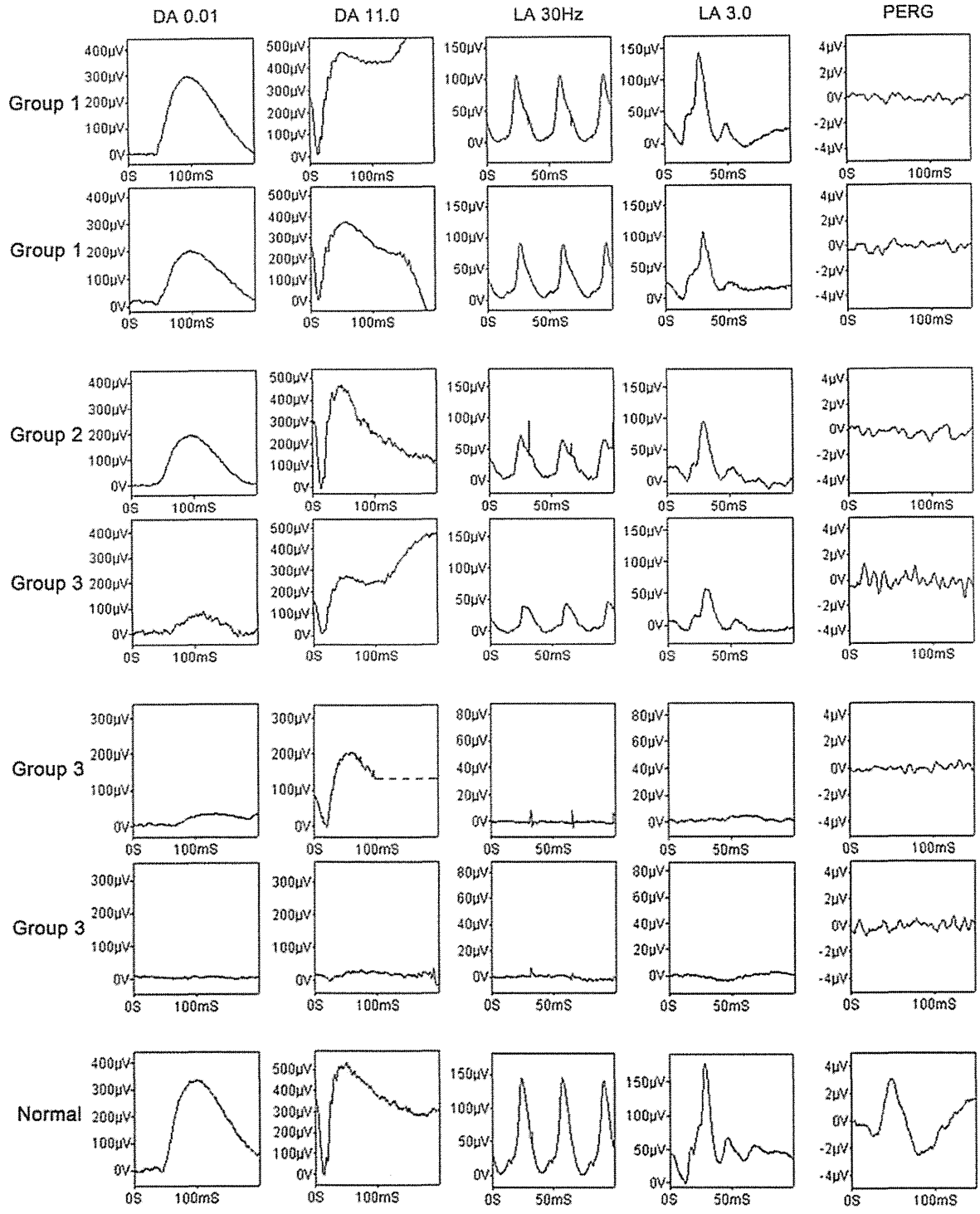

FIGURE 2. Full-field electroretinograms and pattern electroretinograms at baseline and at follow-up from the 3 representative cases of Stargardt disease illustrated in Figure 1 (Patients 17, 42, and 53). Patient 17 demonstrates undetectable pattern electroretinogram (PERG) and normal full-field electroretinograms (ERG) both at baseline (Top row) and at follow-up (Second row), consistent with ERG Group 1 both at baseline and at follow-up. Patient 42 has undetectable PERG and abnormal responses in light-adapted (LA) 3.0, while responses in dark-adapted (DA) 0.01, DA 11.0, and LA 30 Hz are normal at baseline (Third row). At follow-up, all the components of the ERGs are abnormal (Fourth row). Patient 42 demonstrates transition from ERG Group 2 to Group 3, with clinically significant electrophysiologic deterioration observed in rod-derived ERGs. Patient 53 at baseline shows undetectable responses for PERG, LA 30 Hz, and LA 3.0, with abnormal but detectable DA 0.01 and DA 11.0 responses (Fifth row), consistent with ERG Group 3. At follow-up there is only residual ERG activity in the DA 11.0 ERG, representing marked deterioration (Sixth row). (Bottom row) Normal traces are shown for comparison.

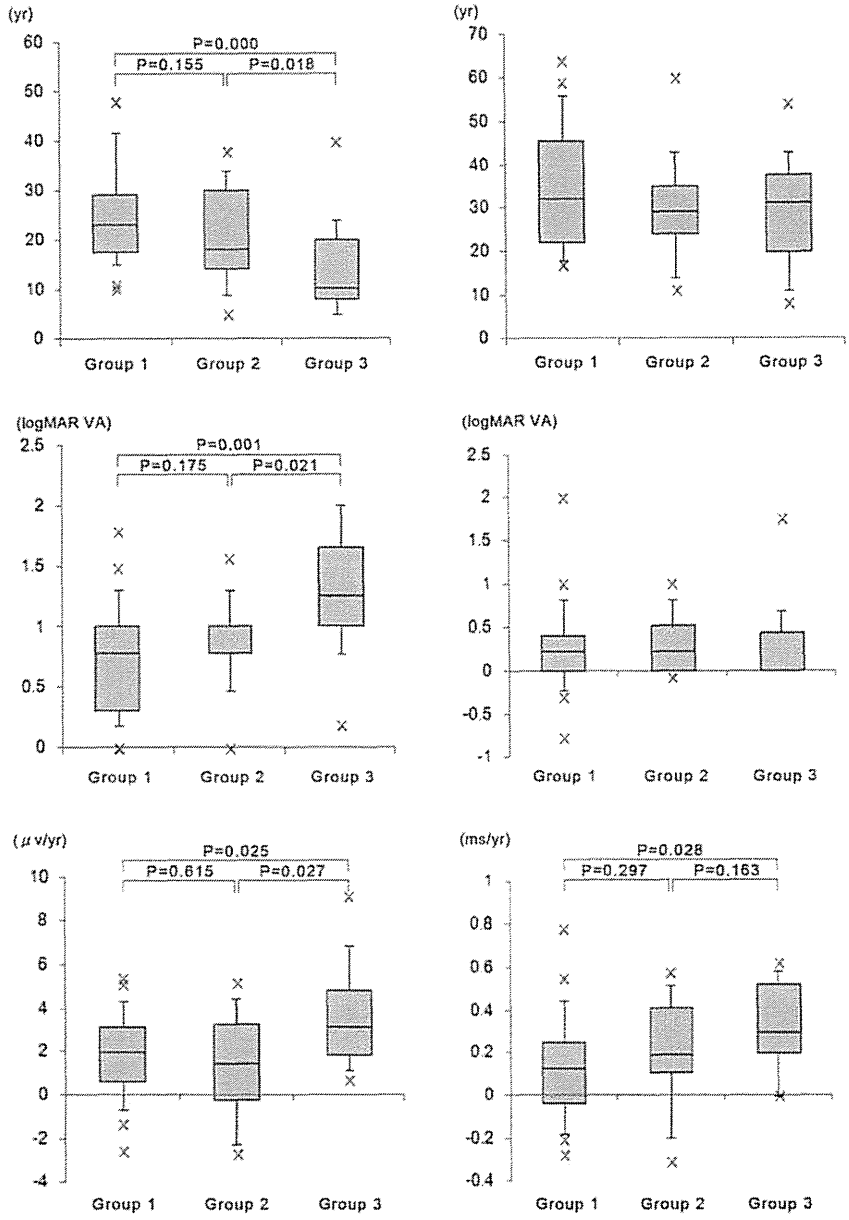

FIGURE 3. A comparison of selected clinical features and electrophysiologic findings associated with each electrophysiologic group at baseline in Stargardt disease, showing significant differences in age of onset, visual acuity at baseline, and electrophysiologic parameters between groups. Age of onset (Top left), age at baseline (Top right), logMAR visual acuity at baseline (Middle left), logMAR visual acuity reduction (Middle right), amplitude reduction per year in the a-wave of the dark-adapted (DA) 11.0 electroretinogram (ERG) (Bottom left), and peak time shift per year in the light-adapted 30 Hz flicker ERG (Bottom right) for the 3 electrophysiologic groups. The boxes show the median and 25% and 75% confidence intervals (lower and upper quartiles). The whiskers extend to what could be considered the 95% confidence interval. Crosses represent values outside the 95% confidence interval. *P* values obtained with the Mann-Whitney *U* test are shown for the parameters in which the Kruskal-Wallis test revealed significant differences. logMAR = logarithm of minimal angle of resolution.

11.0 a-wave and light-adapted 30 Hz of each genotype group are summarized in Tables 3 and 4. There was no statistically significant association identified between the severity of genotype and the extent of electrophysiologic dysfunction on the basis of baseline ERG grouping ($\gamma = -0.126$), although patients with 2 or more non-null variants (genotype B group) less frequently had rod ERG involvement (Table 5 and Supplemental Figure 1).

The distribution of patients with clinically significant electrophysiologic deterioration in each genotype group is

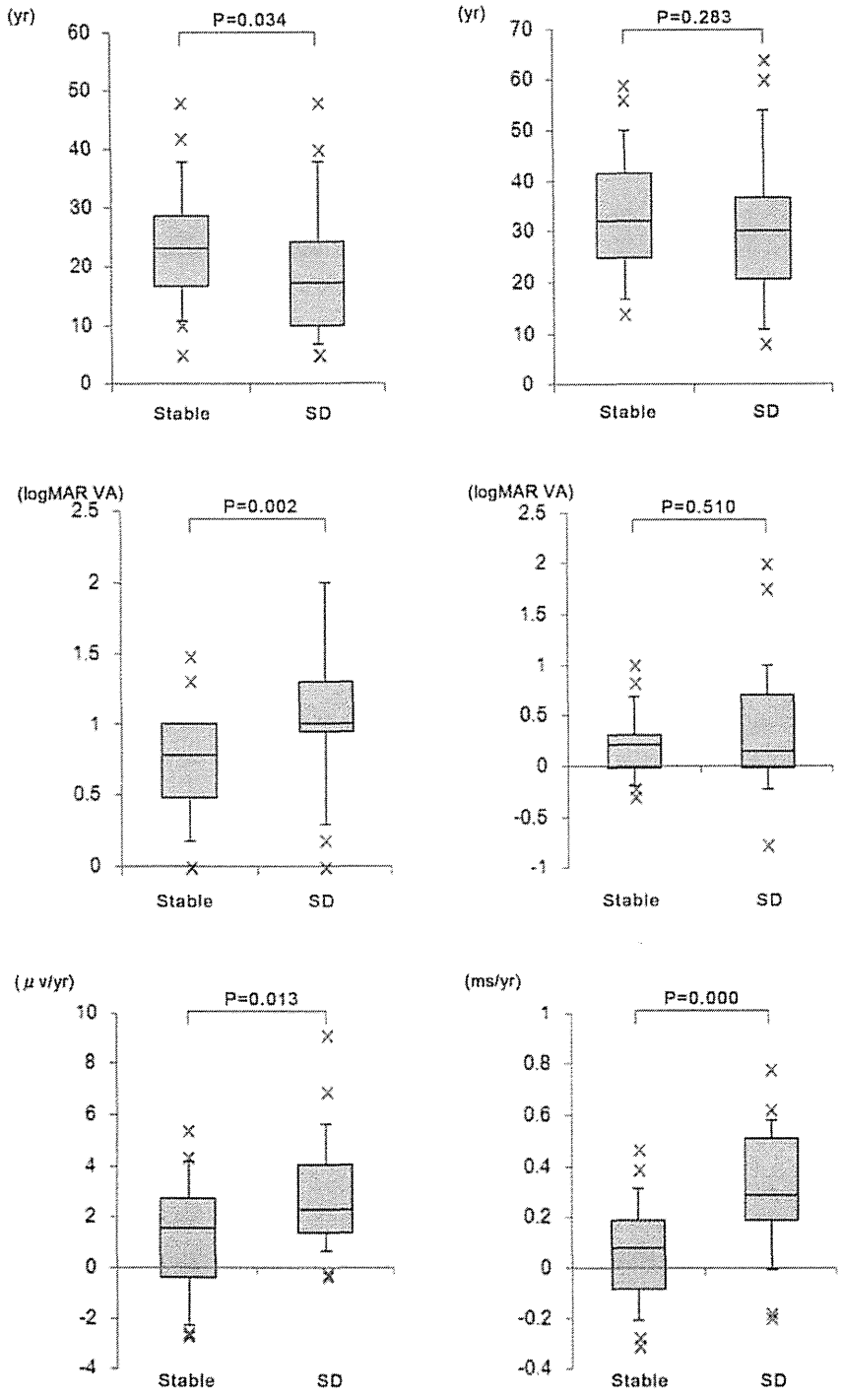

FIGURE 4. A comparison of the clinical findings and electrophysiologic data in Stargardt disease, between the subset of patients with evidence of electroretinogram progression and those without (stable electroretinogram), showing a significant difference in age of onset, visual acuity at baseline, and electrophysiologic parameters between subsets. Age of onset (Top left), age at baseline (Top right), logMAR visual acuity at baseline (Middle left), logMAR visual acuity reduction (Middle right), amplitude reduction per year in the a-wave of the dark-adapted 11.0 electroretinogram (ERG) (Bottom left), and peak time shift per year in light-adapted 30 Hz flicker ERG (Bottom right) for 2 subsets of Stargardt disease (those with and without clinically significant electrophysiologic deterioration). The subset with evidence of clinically significant ERG deterioration is labeled "SD" and the subset without deterioration is labeled "Stable." The boxes show the median and 25% and 75% confidence intervals (lower and upper quartiles). The whiskers extend to what could be considered the 95% confidence interval. Crosses represent values outside the 95% confidence interval. *P* values obtained with the Mann-Whitney *U* test are shown. logMAR = logarithm of minimal angle of resolution.

TABLE 4. Yearly Change[a] in Dark-Adapted Bright Flash Electrophysiologic Responses and Light-Adapted 30 Hz Flicker Responses With Respect to Electrophysiologic Group at Baseline, Electrophysiologic Deterioration, and Genotype Group, in 59 Subjects With Stargardt Disease

	Dark-Adapted 11.0 A-wave			Light-Adapted 30 Hz		
	Amplitude Reduction (μV/y)	Percentage Reduction (%/y)	Peak Time Shift (ms/y)	Amplitude Reduction (μV/y)	Percentage Reduction (%/y)	Peak Time Shift (ms/y)
Group 1 (n = 27)	5.5	1.7	0.10	2.7	2.2	0.14
Group 2 (n = 17)	4.5	1.5	0.09	1.1	1.7	0.19
Group 3 (n = 15)	4.9	3.6	0.18	1.5	3.1	0.32
Stable (n = 27)	3.9	1.2	0.04	2.2	1.9	0.07
Electrophysiologic Deterioration (n = 32)	6.0	2.9	0.18	1.7	2.7	0.31
Genotype A (n = 19)	6.5	3.0	0.14	2.3	3.0	0.23
Genotype B (n = 10)	2.3	0.5	-0.01	1.4	0.9	0.12
Genotype C (n = 18)	5.4	2.1	0.16	2.4	3.1	0.33
Genotype D (n = 12)	4.3	2.1	0.09	1.1	0.9	−0.04
Total (n = 59)	5.1	2.1	0.11	1.9	2.3	0.19

Dark-adapted 11.0 = dark-adapted bright flash electroretinogram (flash intensity 11.0 candela seconds (cd·s)/m^2); Light-adapted 30 Hz = light-adapted 30 Hz flicker electroretinogram (flash intensity 3.0 cd·s/m^2).

[a]A yearly amplitude reduction and a yearly percentage reduction were calculated by dividing the amplitude reduction or the percentage reduction by the follow-up time. A yearly peak time shift (difference between peak time at baseline and follow-up) was also calculated by dividing by the follow-up time.

TABLE 5. Distribution of the 4 Genotype Groups With Respect to Electrophysiologic Group at Baseline and Electrophysiologic Deterioration in Stargardt Disease

	Genotype A	Genotype B	Genotype C	Genotype D
Group 1 (n = 27)	8	5	9	5
Group 2 (n = 17)	4	4	4	5
Group 3 (n = 15)	7	1	5	2
Stable (n = 27)	6	9	7	5
Electrophysiologic deterioration (n = 32)[a]	13	1	11	7
Total (n = 59)	19	10	18	12

[a]The subset without evidence of significant deterioration is described as "Stable."

shown in Table 5 and Supplemental Figure 2 (available at AJO.com). Statistical analysis revealed a significant difference between genotype groups A and B and between genotype groups A and C in terms of age of onset. There was also a statistically significant difference between genotype groups A and B with respect to yearly amplitude reduction of dark-adapted 11.0 a-wave and light-adapted 30 Hz yearly peak time shift (Supplemental Table 5). No statistically significant difference was seen between genotype groups and the other ERG parameters (Supplemental Table 5).

Interestingly, 8 of the 9 patients harboring the variant c.5461-10 T>C (Patients 5, 25, 36, 39, 48, 50, 53-55) had clinically significant ERG progression. All 3 unrelated patients (1, 5, and 31) harboring p.Arg943Gln also had p.Gly863Ala, suggesting linkage disequilibrium of these 2 substitutions, with none of these subjects having clinically significant ERG deterioration.

DISCUSSION

THIS REPORT ADDRESSES LONGITUDINAL CHANGES IN CLINical and electrophysiologic features of Stargardt disease in a large, well-characterized cohort of patients, with 1 or both likely disease-causing *ABCA4* alleles identified in 80% of subjects (47/59). The findings confirm the prognostic value of ERG suggested by earlier cross-sectional data and are relevant to the design of future clinical trials.

Approximately one-fifth of Group 1 patients (dysfunction confined to the macula) progressed to either Group 2 or Group 3 (generalized retinal dysfunction) over a mean time period of 10.5 years, whereas 47% of subjects with Group 2 ERG at baseline changed to Group 3 over the same time period. Overall, there was clinically significant electrophysiologic deterioration in 54% of all patients (32/59), with progression in 22% (6/27) of Group 1 subjects, 65% (11/17) of Group 2, and 100% (15/15) of Group 3. These ERG changes far exceed estimates of normal age-related ERG decline.[39] Thus all patients with initial rod involvement (Group 3) demonstrated clinically significant electrophysiologic deterioration, but only 22% of the patients with normal ERGs (Group 1) at baseline showed clinically significant progression.

A transition in ERG group was seen in 14 patients, with all 14 also meeting the criteria for clinically significant

electrophysiologic deterioration. The 3 patients who progressed from Group 1 to Group 2 had abnormal light-adapted 30 Hz ERGs without any abnormalities in light-adapted 3.0 ERGs; the 30 Hz flicker ERG is known to be a more sensitive indicator of altered cone function than the single-flash photopic ERG. In contrast, both cone full-field ERGs were abnormal in the 3 patients who progressed from Group 1 to Group 3. All 6 patients had a >3 ms peak time shift over time; careful observation of the light-adapted 30 Hz ERGs is important in monitoring Stargardt disease patients with normal ERGs. All but 1 patient with abnormalities in dark-adapted 0.01 or dark-adapted 11.0 had abnormal cone responses, suggesting that generalized cone system dysfunction precedes generalized rod system dysfunction, as has previously been demonstrated.[31]

All 5 patients with undetectable cone responses at follow-up had a >50% amplitude reduction in dark-adapted 11.0 during follow-up. Four patients still had residual responses in dark-adapted 11.0 at follow-up and 1 patient had residual responses in dark-adapted 11.0 at baseline, which became undetectable at follow-up. These findings lend further support to the belief that generalized cone system function is abolished before generalized rod system loss, and that the amplitude of dark-adapted 11.0 responses may be helpful in assessing residual retinal function in cases with very severe retinal dysfunction.

The clinical characteristics of each ERG group showed a statistically significant difference between Groups 1 and 3 and Groups 2 and 3 in terms of age of onset, in keeping with the original cross-sectional data, with a younger age of onset associated with more generalized retinal dysfunction.[31] There was also a statistically significant difference in logMAR VA between Groups 1 and 3 and Groups 2 and 3, with worse VA associated with increasingly severe generalized retinal dysfunction, as has been previously proposed.[31] No statistically significant differences were observed between groups with respect to other parameters, including age at baseline, duration of disease, and interval of follow-up. In addition, the age of onset was earlier in subjects who had clinically significant ERG progression compared to those who did not meet criteria for clinically significant deterioration, further supporting the likelihood that age of onset in Stargardt disease is of prognostic value.[7] For ease of comparison between groups, a linear longitudinal relationship has been assumed and the rate of change expressed in terms of yearly amplitude reduction, yearly percentage reduction, and yearly peak time shift. This study has not examined the linearity of change between baseline and follow-up testing; a prospective study with additional, more frequent time point sampling will help address this pertinent question. It is likely that progression will be linear in some individuals and nonlinear in others, in keeping with the commonplace phenotypic heterogeneity of inherited retinal disorders.

ABCA4 mutations were originally reported in patients with autosomal recessive Stargardt disease but shortly thereafter were identified in association with cone dystrophy, cone-rod dystrophy, and "retinitis pigmentosa," with a genotype-phenotype relationship having been proposed.[10,13–15,21,24,40–43] In the present cohort, 82% of patients (22/27) in ERG Group 1 at baseline, 70% (12/17) in Group 2, and 87% (13/15) in Group 3 harbored at least 1 *ABCA4* variant.

A likely disease-causing *ABCA4* variant was identified in 47 out of 59 patients, with 6 putative novel mutations detected. There was no statistically significant association identified between the category of genotype and the extent of electrophysiologic dysfunction on the basis of ERG group, although patients with 2 or more non-null variants (genotype B group) less frequently had rod ERG involvement. A statistically significant greater percentage of patients with null variants (genotype A group) (68%, 13/19) had ERG deterioration, in comparison with patients harboring 2 or more non-null variants (10%, 1/10), with the majority therefore having a stable ERG (90%, 9/10). There was also a statistically significant difference between genotype groups A and B with respect to yearly amplitude reduction of dark-adapted 11.0 a-wave and light-adapted 30 Hz yearly peak time shift. There are several factors that may account for the relative lack of more clearly demonstrable genotype-phenotype correlations, including the relatively small sample size, the fact that only 1 disease-causing allele was identified in most cases, and the vast allelic heterogeneity of *ABCA4*. However, one particular variant (c.5461-10T>C) was found to be associated with electrophysiologic progression. This mutation has been previously reported to be associated with severe disease in both the homozygous and compound heterozygous states,[42,44] suggesting that it may be a marker for more severe disease, which is likely to show clinically significant progression.

Co-inheritance of p.Arg943Gln and p.Gly863Ala has been previously reported,[44,45] with p.Arg943Gln thought to be a benign polymorphism[29,45] and p.Gly863Ala believed to be associated with milder phenotypes,[42,45] although there has been a single report of a severe phenotype associated with p.Gly863Ala in the homozygous configuration.[44] Only 2 out of 8 patients harboring p.Gly863Ala in the present series had evidence of ERG progression, suggesting this variant is indeed likely to be associated with milder disease.

The longitudinal study described herein has identified that a patient's allocation to an individual ERG group, as proposed in the original cross-sectional study, may change over time—a conclusion that could not be made previously because of the inherent limitations of a cross-sectional survey. The rate of progression between groups and within groups has been determined, and age of onset and, to a lesser extent, visual acuity may predict the degree of eventual generalized retinal dysfunction and/or progression. It is important that only 20% of those patients with initially normal full-field ERGs showed evidence of progression